Estimating higher-order structure functions from geophysical turbulence time series: Confronting the curse of the limited sample size

Adam W. DeMarco*
Department of Marine, Earth, and Atmospheric Sciences, North Carolina State University, Raleigh, North Carolina 27695, USA

Sukanta Basu
Faculty of Civil Engineering and Geosciences, Delft University of Technology, Delft, the Netherlands
(Received 5 December 2016; revised manuscript received 10 April 2017; published 9 May 2017)

Utilizing synthetically generated random variates and laboratory measurements, we document the inherent limitations of the conventional structure function approach in limited sample size settings. We demonstrate that an alternative approach, based on the principle of maximum likelihood, can provide nearly unbiased structure function estimates with far less uncertainty under such unfavorable conditions. The superiority of this approach over the conventional approach does not diminish even in the case of strongly correlated samples. Two entirely different types of probability distributions, which have been reported in the turbulence literature, are found to be compatible with the proposed approach.

DOI: 10.1103/PhysRevE.95.052114

I. INTRODUCTION

Characterization of small-scale turbulence by higher-order statistical moments has a long and rich history in both laboratory and geophysical settings. Dating back nearly 50 years, Van Atta and Chen [1] conducted an extensive atmospheric boundary layer (ABL) experiment to measure up to fourth-order moments of atmospheric velocity fluctuations over the ocean. Their study revealed some intriguing similarities, and differences, between what was observed and the existing turbulence hypotheses [e.g., Kolmogorov and Obukhov 1941 (KO41) [2,3]]. These findings led to increased efforts (see Refs. [4–10], just to name a few) to acquire extensive measurements of ABL flows in order to further explore the statistical and dynamical features of turbulence (e.g., power-law scaling, nonlinearity in energy cascade). At the same time, researchers in a myriad of other geophysical disciplines, from oceanography (e.g., phytoplankton biomass distribution in turbulent coast waters [11,12]) to magnetohydrodynamics (e.g., intermittency in solar wind fluctuations [13–17]), initiated their own investigations in this intriguing research arena. Due to the lack of modern instrumentation, the majority of the initial studies were conducted solely within the Eulerian framework (by invoking the so-called Taylor's hypothesis). Fortunately, several recent contributions have attempted to fill the void in the Lagrangian framework (see Refs. [18–21] and references therein).

Over the years, the utilization of higher-order statistics not only became common practice for (in)validating various hypotheses against experimental findings, but it also enabled the research community to gain a better understanding of different types of turbulent flows. For example, many studies have been conducted which strive to make a distinction between active and passive scalars [22–24] as well as contrasting atmospheric convection [25,26] from Rayleigh-Bénard convection [27–31]. For other illustrative examples, please refer to the outstanding books by Frisch [32] and Tsinober [33].

In parallel to the analysis and characterization studies, a handful of pioneering works focused on the development of cascade models with the inherent ability to capture the observed higher-order scaling behaviors. These models ranged from a simplistic β-model which seeks to resemble the intermittent behavior of turbulent cascade from a geometric point-of-view [34,35] to a more complex probabilistic model, which describes the energy cascade (multiplicative) process within the inertial range in a multifractal framework [36–38]. Likewise, a number of other simplified dynamical models (e.g., shell models, stochastic Burgers equation) [39–43] were developed to mimic a number of intrinsic traits of three-dimensional turbulence. From our perspective, this line of research is still far from being mature.

It is important to acknowledge that the aforementioned higher-order characterization and related modeling activities are not only of importance from a pedagogical point of view, but they are also beginning to make impacts in diverse practical applications, including (but not limited to) combustion [44,45]; wind energy [46], and atmospheric modeling [47]. We strongly believe that the gamut of applications can be significantly broadened with further analyses of various geophysical data sets. Unfortunately, the typical sample size of such data sets is orders of magnitude fewer than their laboratory counterparts. This disparity in sample size poses a serious challenge for higher-order statistical analyses using the traditional sample moments. In this paper, we advocate an alternative approach to confront this challenge.

II. LIMITED SAMPLE SIZE PROBLEM

It is common knowledge in the turbulence research community that capturing higher-order moments of turbulent variables can be rather difficult without a substantial sample size of experimental data [8,32,48–55]. In particular, the ability to accurately estimate the moments can be directly related to the tails of the underlying probability density function (pdf), which signify rare events [56].

Thus, in laboratory settings, it is customary to measure turbulence with upwards of 10^7 samples using hot-wire

*awdemarc@ncsu.edu

anemometry (sampling rate on the order of several kHz). However, acquisition of hot-wire data in a natural geophysical setting is quite challenging. For example, in the case of ABL field experiments, one needs to perform meticulous hot-wire calibration at short regular intervals in order to account for the ever-changing, diurnally varying ABL flow parameters [57,58]. As a viable alternative, the ABL community widely uses sonic anemometers (sampling rate of ∼20 Hz) for measuring turbulent velocity fields. In contrast to hot wires, these sensors require much less periodic calibration and maintenance. However, these instruments can only collect O(20–40) thousand samples during a measurement time window of 15–30 min. Publications, from as early as the 1970s, pointed out that such short time series are not adequate for estimating moments beyond fourth-order [1,8]. Unfortunately, one cannot circumvent this problem by simply using longer time records owing to the frequent interference of nonstationary and nonturbulent motions (a.k.a. mesoscale motions). An earlier work attempted to tackle this problem using cumulants [59]. It was demonstrated that a cumulant-based approach can reliably estimate the so-called intermittency exponent [32] from short ABL time series. However, the cumulants involve logarithmic functions of the velocity increments; as such, they are more influenced by the peak of the pdf rather than its tails. Thus, their usage in the estimation of higher-order moments is questionable. As an alternative, in this paper, we illustrate a maximum likelihood-based moment estimation technique which can provide statistically accurate higher-order moments from relatively short geophysical series.

III. QUANTIFYING UNCERTAINTY IN STRUCTURE FUNCTION ESTIMATES

It is customary to quantify the behavior of fine-scale fully developed turbulence, using structure function (SF) analysis:

$$S_p = \langle |u(x+r) - u(r)|^p \rangle = \langle |\delta u|^p \rangle \sim r^{\zeta p}, \qquad (1)$$

where S_p is the pth-order SF with respect to the spatial separation (or increment), r. The angular brackets here indicate spatial averaging, $|\delta u|^p$ is the pth-order absolute moment of the velocity increments, and ζ_p is the scaling exponent.

Many laboratory and geophysical turbulence studies have shown that the pdfs of velocity increments, pdf[δu], are scale-dependent and change steadily within the inertial subrange. Specifically, these distributions have shown to exhibit strong non-Gaussian behavior at small increments, then become more Gaussian as separation increases [15,56,61–65]. A few years ago, Barndorff-Nielsen *et al.* [56] demonstrated that the normal inverse Gaussian (NIG) distribution has the inherent ability to capture such scale-dependent traits in a parsimonious manner. An illustrative example is shown in Fig. 1. Here, following the approach by Rydberg [60], we have numerically generated three NIG distributed variates with different parameter settings. This figure clearly attests to the fact that the NIG distribution can indeed capture heavy-tailed (●), moderate-tailed (▲), and near-Gaussian (■) distributions with appropriate choice of parameters. More details regarding the NIG distribution are provided in Appendix A.

Next, using the NIG distributed variates, we quantify the impacts of pdf shapes and sample sizes on the uncertainty of

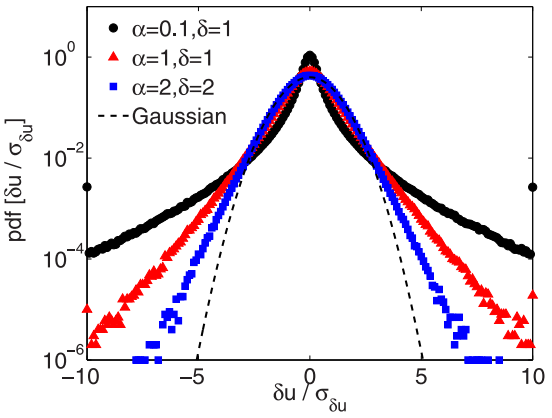

FIG. 1. NIG distributed variates with three different parameter combinations: (a) $\alpha = 0.1, \delta = 1$, (b) $\alpha = 1, \delta = 1$, and (c) $\alpha = 2, \delta = 2$. For all these cases, the parameters μ and β are assumed to be equal to zero. Please refer to Appendix A for a detailed description of the NIG parameters. For each case, 10^7 samples were generated using Rydberg's algorithm [60]. The distributions were normalized by the standard deviation $\sigma_{\delta u}$. A Gaussian pdf is overlaid (dashed line) as a reference.

the SF estimates. We consider a wide range of sample sizes (N) from 10^3 to 10^7 for each of the three pdfs shown in Fig. 1. In order to obtain reliable statistics, we generate 100 realizations for each case. Based on the numerically generated variates, we compute SF using Eq. (1). Without loss of generality, we focus on the sixth-order SF (S_6).

The decision to consider S_6 as a test statistic was not arbitrary. In turbulence literature, there is considerable interest in the accurate estimation of S_6, since its scaling exponent is directly used to determine the intermittency exponent, $\mu^* \equiv 2 - \zeta_6$, which relates to the behavior of the underlying non-Gaussian distributions.

The estimated (henceforth "empirical") S_6 values are shown in Fig. 2 utilizing a standard box-plot notation where 50% of the data lie within the blue "box" and the red line segment within the "box" is the median value of the data. The "whiskers" (i.e., the vertical dashed line segments) correspond to $\pm 2.7\sigma$, while the + are the outliers. The following observations can be made based on this figure:

(1) For all the cases, with increasing sample size the S_6 estimates converge towards the true values as would be expected.

(2) For comparable sample size, the uncertainty of the S_6 estimate is much higher for the heavy-tailed case than the near-Gaussian case; the moderate-tailed case falls in between.

(3) For small sizes, the S_6 estimates are strongly biased for the heavy-tailed case. The bias decreases for the moderately tailed case, while for the near-Gaussian case, the estimates are close to unbiased.

These findings have significant implication on geophysical data analyses and require scrutiny in to whether a collection of samples are robust enough to provide an accurate estimation of a specific higher-order moment. In a recent paper, Dudok de Wit [66] made an interesting contribution in this arena by borrowing ideas from the Extreme Value (EV) theory. He proposed a simple approach to compute the maximum moment

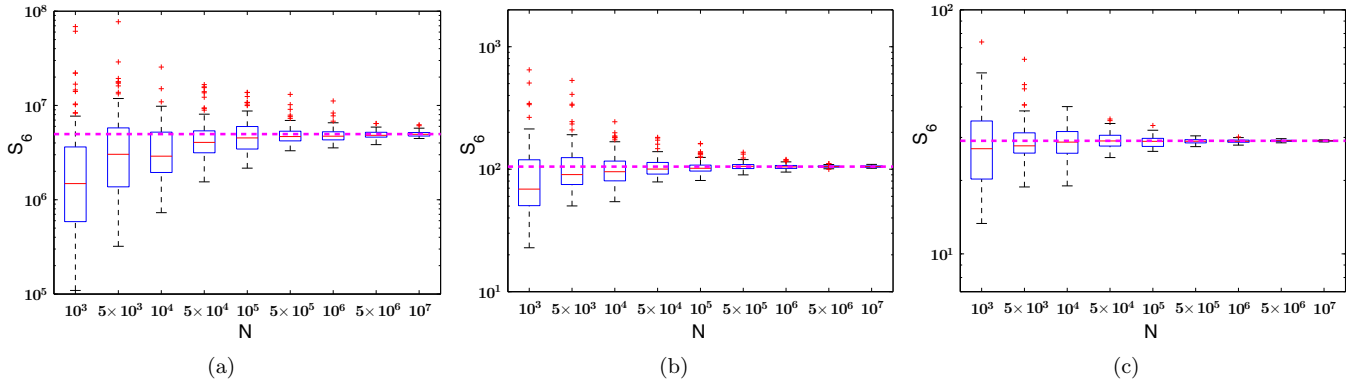

FIG. 2. "Empirical" S_6 box plots for three different NIG distributions with parameter combinations: (a) $\alpha = 0.1, \delta = 1$, (b) $\alpha = 1, \delta = 1$, and (c) $\alpha = 2, \delta = 2$. The parameters μ and β are assumed to be equal to zero. The sample sizes (N) are varied from 10^3 to 10^7. One hundred realizations are used for the construction of the box plots. The dashed magenta lines represent the true S_6 values based on Eq. (A4).

order ($p_{\max}$) for which reliable estimation of structure function ($S_{p_{\max}}$) is feasible for a given spatial or time series. In the following section, using the aforementioned NIG distributed variates, we elaborate on Dudok de Wit's approach followed by a recommendation for certain improvement.

IV. ESTIMATING $p_{\max}$ FROM LIMITED DATA

Let us denote the rank-ordered (in decreasing order) absolute value of the velocity increments as: $\Phi_k = |\delta u|_k / \sigma_{\delta u}$, where $k = 1, \ldots, N$. Dudok de Wit [66] showed that for small values of k, Φ_k versus k follows the well-known Zipf power-law behavior:

$$\Phi_k \propto \left(\frac{k}{N}\right)^{-\gamma^*}, \tag{2}$$

where γ^* is known as the tail index (a.k.a. shape parameter). Via analytical derivations (with one minor approximation), Dudok de Wit [66] related γ^* to $p_{\max}$ as follows:

$$p_{\max} = \left\lfloor \frac{1}{\gamma^*} \right\rfloor - 1, \tag{3}$$

where the floor bracket denotes the integer part.

In Fig. 3 the rank-ordered plots for three NIG distributed variates are shown. In these log-log plots, the power-law behavior is clearly discernible for small values of k. Following Dudok de Wit's approach, γ^* values are estimated using ordinary linear regression over the range of $10 \leqslant k \leqslant 1000$. These values along with the estimated $p_{\max}$ values are reported in Table I.

As shown in Ref. [66], and illustrated here in Table I, there is a clear dependence on $p_{\max}$ values for the various sample sizes. Additionally, we also notice that the shape of the pdfs directly influences $p_{\max}$. For instance, in the case of the heavy-tailed distribution ($\alpha = 0.1$ and $\delta = 1$), a minimum sample size of 10^7 is required in order to provide a reliable estimate of S_6. However, for a near-Gaussian distribution ($\alpha = 2$ and $\delta = 2$), only 10^5 samples will suffice. We would like to note that these results are in complete agreement with the ones reported in Fig. 2.

Even though the overall approach of Dudok de Wit [66] is quite elegant and powerful, the tail index estimation component is rather subjective and not statistically robust. It can be significantly improved by employing one of the well-tested estimators from the field of EV theory [67] instead of using linear regression. Over the years, several estimators for γ^* have been proposed in the literature, including (but not limited to) Pickand's estimator [68], Hill estimator [69], and the Dekkers-Einmahl-de Haan estimator [70]. In this work, we

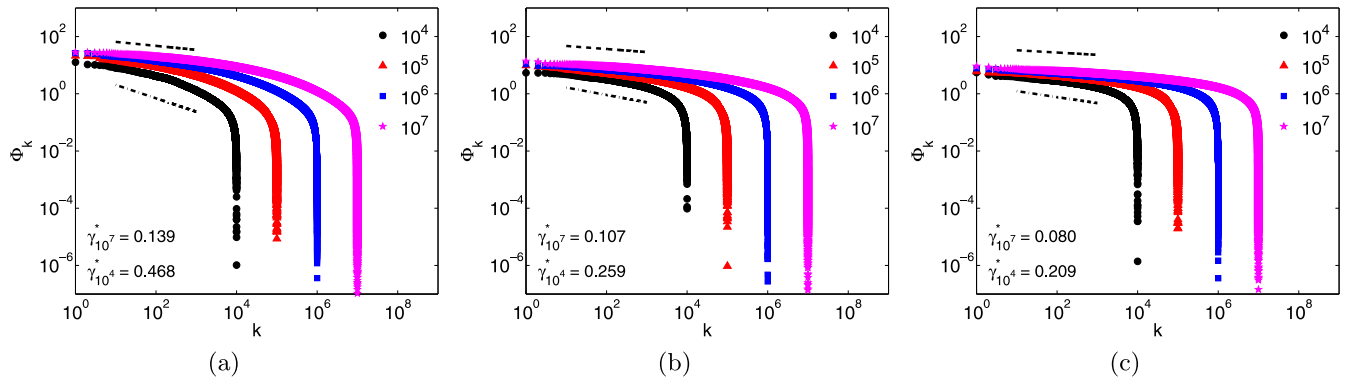

FIG. 3. Rank-order (a.k.a. Zipf) plots for NIG distributed variates with three different parameter combinations: (a) $\alpha = 0.1, \delta = 1$, (b) $\alpha = 1, \delta = 1$, and (c) $\alpha = 2, \delta = 2$. The parameters μ and β are assumed to be equal to zero. The sample sizes (N) are varied from 10^4 to 10^7. The tail indices (γ^*) are estimated for $N = 10^4$ (dot-dashed) and $N = 10^7$ (dashed) and reported in the bottom-left corner of the plots.

TABLE I. Tail-index (γ^*) and maximum moment order ($p_{\max}$) for NIG distributed variates of varying sample sizes and with three different parameter combinations.

	$\alpha = 0.1, \delta = 1$		$\alpha = 1, \delta = 1$		$\alpha = 2, \delta = 2$	
N	γ^*	$p_{\max}$	γ^*	$p_{\max}$	γ^*	$p_{\max}$
5×10^3	0.583	0	0.346	1	0.265	2
1×10^4	0.468	1	0.259	2	0.209	3
5×10^4	0.344	1	0.206	3	0.157	5
1×10^5	0.294	2	0.185	4	0.140	6
5×10^5	0.213	3	0.146	5	0.117	7
1×10^6	0.204	3	0.130	6	0.109	8
5×10^6	0.155	5	0.109	8	0.088	10
1×10^7	0.139	6	0.107	8	0.080	11

use the popular Hill estimator:

$$\gamma^* = \left[\frac{1}{k} \sum_{i=1}^{k} \log \left(\frac{\Phi_i}{\Phi_{k+1}} \right) \right]^{-1}, \tag{4}$$

where $k = 1, \ldots, N-1$. It is customary to estimate γ^* value through a graphical representation called a Hill plot. This type of depiction is formed by plotting γ^* versus k [71]. For EV distributions (e.g., Pareto), estimated γ^* (or, related $p_{\max}$ via Eq. (3)) are expected to stabilize (i.e., exhibit nonfluctuating behavior) with increasing values of k.

To illustrate this technique, we present, in Fig. 4, Hill plots using the same three NIG distributed variates and range of sample sizes as in Fig. 3. Even though it captures heavy tails [72], a NIG distribution is not formally an EV distribution. Thus, perfect stabilization of the Hill plots is not anticipated. Nonetheless, Fig. 4(a) shows that all four curves smoothly and slowly decrease below the dashed line, representing $p_{\max} = 6$. This behavior indicates that, for this particular heavy-tailed distribution, even with 10^7 samples we cannot provide an accurate estimation of S_6. However, as the pdf shapes are modified and tend to become more Gaussian, the Hill plots [Figs. 4(b) and 4(c)] reveal that higher order moments are achievable for smaller sample sizes. Another important feature that Fig. 4 portrays is that sixth-order moment estimations pose issues with sample size less than 10^5 irrespective of the shape of the distribution. In fact, this characteristic can also be seen through the "empirical" sixth-order SF calculations displayed in Fig. 2.

In summary, the approach proposed by Dudok de Wit [66] and our suggested modification provide guidelines into the $p_{\max}$ values attainable by the conventional structure function analysis. In the next section, we advocate an alternative approach, based on maximum likelihood estimation (MLE), which has the ability to reliably compute structure functions well beyond $p_{\max}$. However, to employ such an approach, one needs to make an assumption about the underlying pdf of the velocity increments. In the present work, we assume it to be following the NIG distribution [56].

V. MAXIMUM LIKELIHOOD-BASED STRUCTURE FUNCTION ESTIMATION

If the velocity increments follow the NIG distribution, the structure functions can be rewritten as

$$S_p = E\left(|x^p|\right) = \int_{-\infty}^{\infty} |x|^p f_{\mathrm{NIG}}(x; \alpha, \beta, \mu, \delta) dx. \tag{5}$$

In this case, x equals δu. If the parameters of the NIG distribution are known (or estimated), one can simply use a numerical integration approach to compute the integral.

However, in a typical laboratory or geophysical setting, these NIG parameters are not known *a priori*. One can then use the method of moments approach (see Appendix A) to estimate them, but this technique has been shown to be unstable [73]. A more robust approach would be to use the maximum likelihood estimator (MLE; [74,75]), for details see Appendix B. Since MLE is a computationally very expensive technique and occasionally requires numerous iterations for convergence, in this work we make use of the MME-based estimates as the initial conditions for the MLE computations.

In order to illustrate the superiority of MLE over MME, we make use of the Kolmogorov-Smirnov (K-S) statistic based on the empirical distribution function (EDF; [76]):

$$D = \sup_x |F_{\mathrm{EMP}}(x) - F_{\mathrm{NIG}}(x)|, \tag{6}$$

where F_{EMP} and F_{NIG} are the empirical and estimated NIG distribution functions, respectively. The results associated with a heavy-tail distribution ($\alpha = 0.1, \delta = 1$) are shown in Fig. 5.

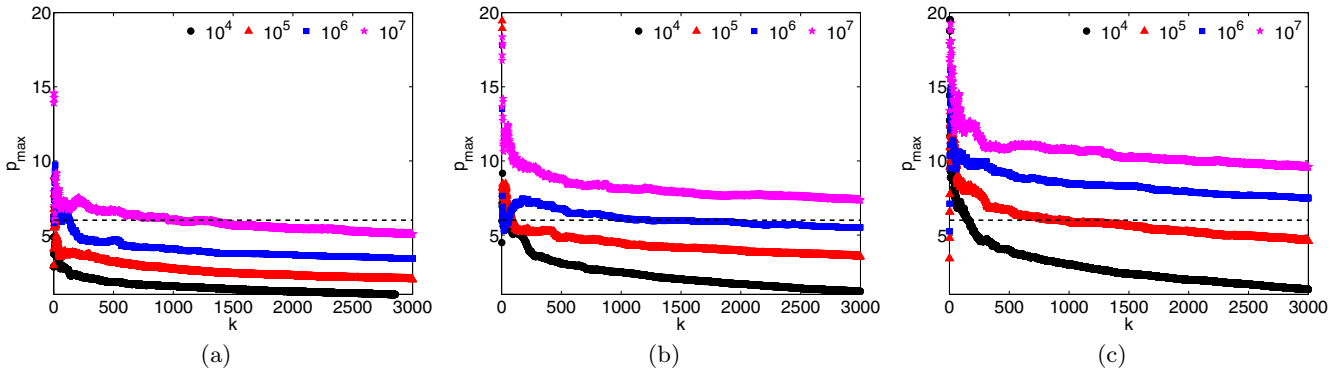

FIG. 4. Hill plots for NIG distributed variates with three different parameter combinations: (a) $\alpha = 0.1, \delta = 1$, (b) $\alpha = 1, \delta = 1$, and (c) $\alpha = 2, \delta = 2$. The parameters μ and β are assumed to be equal to zero. The sample sizes (N) are varied from 10^4 to 10^7. The dashed black lines represent $p_{\max} = 6$.

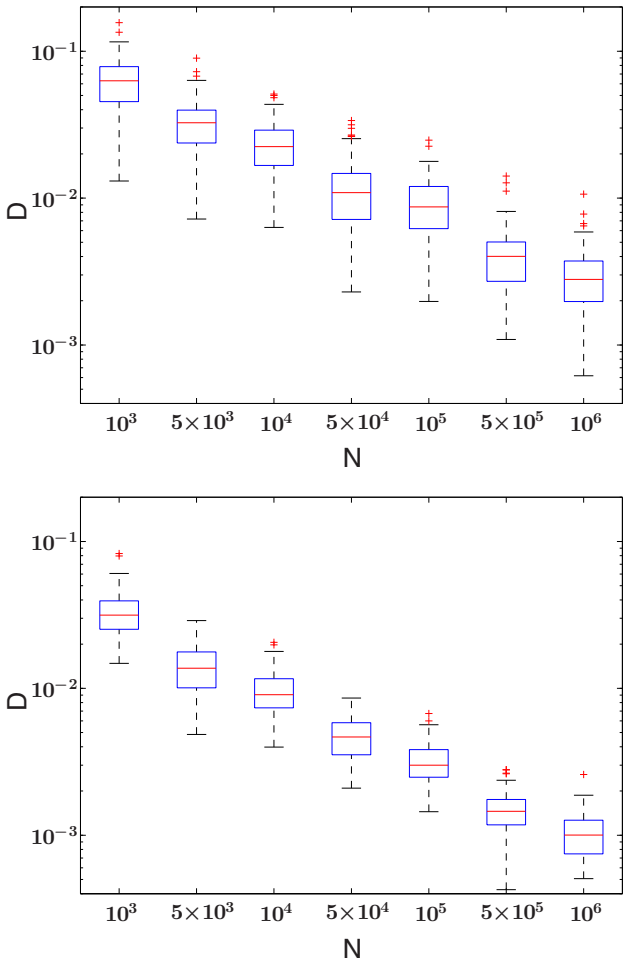

FIG. 5. Box plots of K-S test statistic (D) comparing MME (top panel) versus MLE (bottom panel) results. The following parameters are utilized to generate the random variates: $\alpha = 0.1$, $\beta = 0$, $\mu = 0$, and $\delta = 1$ (heavy-tailed). The sample sizes (N) are varied from 10^3 to 10^6. As before, 100 realizations are used for the construction of the box plots.

Without any doubt, for all sample sizes, MLE outperforms MME by having (i) lower (median) values of D and (ii) reduced uncertainty bounds of D. Similar comparative results were obtained for moderate-tail and near-Gaussian pdfs as well (not shown here for brevity).

Within the MLE computation, we explored two types of numerical algorithms: Expectation-Maximization (E-M) [77] and Nelder-Mead method [78]. Both these approaches produced near-identical results (up to the fourth decimal points). Our implementation of the E-M algorithm follows Ref. [74]. We chose this specific approach due to its simplicity and robustness for the NIG distribution. A pseudocode is included in Appendix B. For the Nedler-Mead method, we used a commercial MLE function from MATLAB. Further details regarding this approach can be found in Ref. [79].

Using the idealized NIG distributed variates generated in Fig. 2, we now apply the MLE approach to find out if an improvement over the conventional approach is feasible. The MLE-based S_6 estimates are displayed in Fig. 6 using the standard box-plot notation as before. Of note, the sample size range is reduced from 10^7 in Fig. 2 to 10^6 in Fig. 6 since MLE provides converged statistics with far fewer data samples.

There are distinct differences in results between Fig. 2 and Fig. 6. First of all, for all sample sizes and pdf shapes, the estimated S_6 values are nearly unbiased in Fig. 6. Second, the uncertainty bounds are significantly reduced in Fig. 6 in comparison to the corresponding box plots in Fig. 2. In other words, the MLE-based structure function approach is much more robust and more reliable in comparison to the conventional structure function approach, especially in a small sample setting.

In the following section, we will investigate if this conclusion also holds in the case of correlated and real-data samples.

VI. EFFECTS OF CORRELATION

To this point, our analysis has been focused on independent and identically distributed (i.i.d) random NIG variates. However, in practice, the samples may be correlated. For example, in the case of velocity increments, Anselmet *et al.* [49] and Huang *et al.* [80] reported scale-dependent temporal correlations. In order to quantify the impact of correlation on higher-order moment estimation, we synthetically generated 100 realizations of correlated NIG variates. Each realization is created via the following steps:

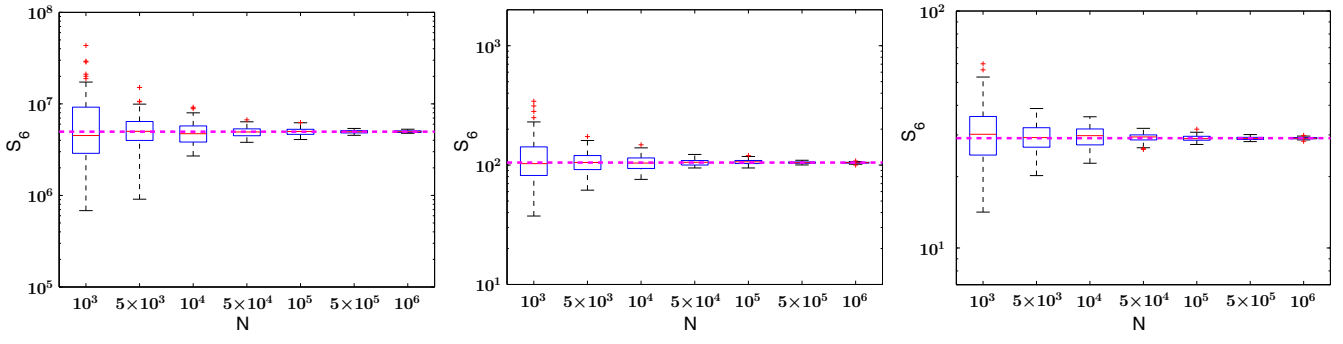

FIG. 6. MLE-based S_6 box plots for three NIG distributions with parameter combinations: (a) $\alpha = 0.1, \delta = 1$, (b) $\alpha = 1, \delta = 1$, and (c) $\alpha = 2, \delta = 2$. The parameters μ and β are assumed to be equal to zero. The sample sizes (N) are varied from 10^3 to 10^6. One hundred realizations are used for the construction of the box plots. The dashed magenta lines represent the true S_6 values based on Eq. (A4).

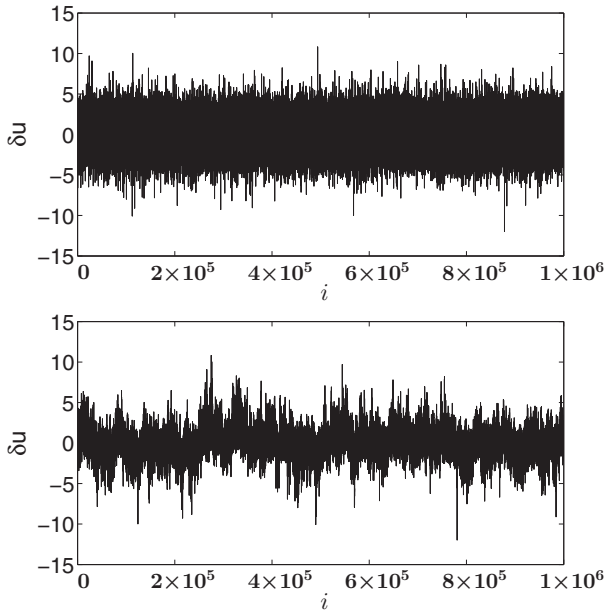

FIG. 7. Realizations of i.i.d (top panel) and correlated (bottom panel) NIG variates. Both realizations follow the same NIG distribution with prescribed parameters: $\alpha = 1$, $\beta = 0$, $\mu = 0$, and $\delta = 1$.

(1) As before, generate i.i.d NIG variates (sample size of one million) using the approach by Rydberg [60]. We assumed a moderate-tailed distribution ($\alpha = 1$, $\beta = 0$, $\mu = 0$, and $\delta = 1$).

(2) Generate a red-noise series (sample size of one million) with a spectral slope between zero and minus 1. The magnitude of this slope is randomly selected from a uniform distribution.

(3) Perform simple histogram matching between the i.i.d NIG series and the red-noise series. The resultant series preserves the NIG pdf accurately, and it is correlated. However, it does not follow the exact correlation structure of the red noise.

Illustrative examples of i.i.d and correlated NIG variates are shown in Fig. 7. Even though they look distinctly different (due to correlation structure), both realizations follow an identical pdf.

Let us denote each of the 100 correlated NIG realizations as $\delta u_1^{(k)}, \ldots, \delta u_M^{(k)}$; where $M = 10^6$ and k varies from 1 to 100. From each realization, we extract a contiguous subset $\delta u_i^{(k)}, \ldots, \delta u_{i+N-1}^{(k)}$, where $i \geqslant 1$ and $i + N - 1 \leqslant M$. We vary the subsample size N from 10^3 to 10^6. Since we have a total of 100 realizations, for a specific value of N, we also get 100 subsamples. These subsamples are used to estimate S_6 using the aforementioned "empirical" and MLE approaches. These results are shown in Fig. 8.

Comparing the results from Fig. 8 to the corresponding box plots in Fig. 2, it is clear that the uncertainty bounds have significantly increased for the correlated samples. Also, the number of outliers have increased substantially. Still, for this difficult scenario, the MLE-based estimates outperforms the "empirical" ones in terms of bias and uncertainty bounds. It is quite remarkable that for all sample sizes, the MLE-based estimates are unbiased. It is needless to say that both the estimates do converge to the true S_6 value for large sample sizes; however, the convergence is slower than the i.i.d scenario.

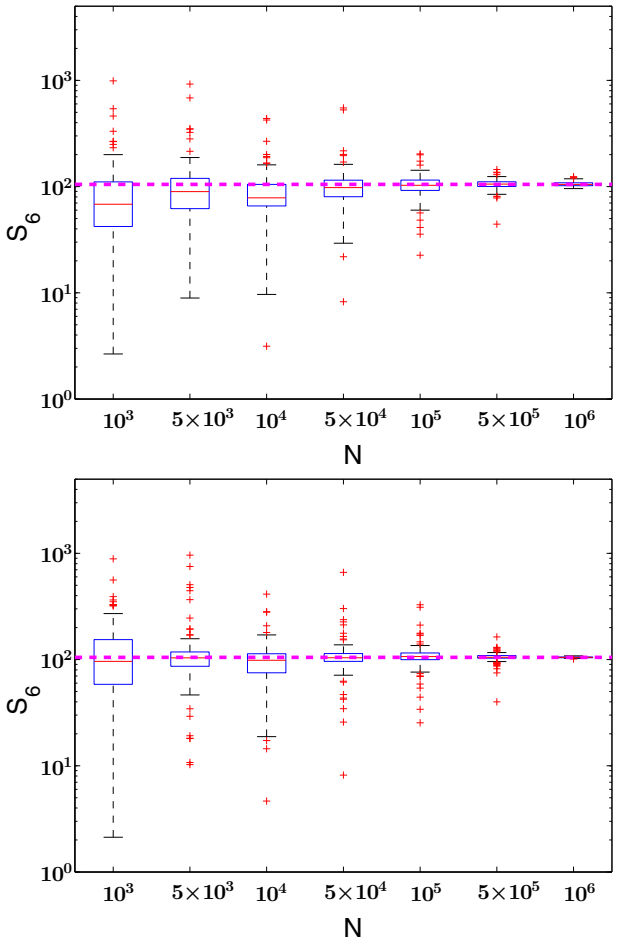

FIG. 8. "Empirical" (top panel) and MLE-based (bottom panel) S_6 box plots for correlated NIG variates. The following parameters are utilized to generate the random variates: $\alpha = 1$, $\beta = 0$, $\mu = 0$, and $\delta = 1$. The sample sizes (N) are varied from 10^3 to 10^6. One hundred realizations are used for the construction of the box plots. The dashed magenta lines represent the true S_6 value based on Eq. (A4).

VII. WIND TUNNEL DATA

To further showcase the strength of the MLE approach, we utilize laboratory data from the Office National d'Etudes et de Recherches Aérospatiales (ONERA) S1 wind tunnel. These velocity measurements were obtained with a DISA 55M01 constant temperature system with Wollaston wire (3 mm diameter and 0.35 mm length for all the air flows). The sample size for this data is approximately ($\sim 13 \times 10^6$) long with a sampling rate of 25 kHz. Following the conventional turbulence analysis techniques, we have invoked Taylor's hypothesis to convert this time series to a spatial series and normalized the original series to have zero mean and unit standard deviation. For further details on this data set and past ONERA S1 wind tunnel experiments, please refer to Refs. [81–83].

Figures 9(a) and 10(a) depict pdfs of velocity increments for two specific Δt values: 4×10^{-4} sec and 1.35×10^{-2} sec, respectively. Given their distinctly different tail behavior,

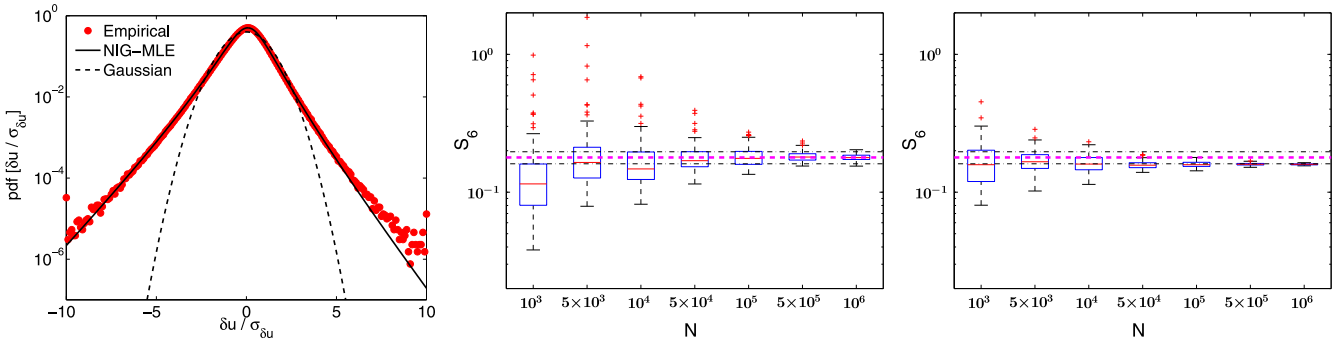

FIG. 9. Analyses of ONERA S1 wind tunnel data. Selected increment: $r = 8.2$ mm or $\Delta t = 4 \times 10^{-4}$ sec, (a) corresponding PDF with NIG-MLE fit, (b) "Empirical" S_6 box plots, (c) NIG-MLE S_6 box plots. One hundred realizations are used for the construction of the box plots. The dashed magenta line represent the S_6 values based on Eq. (1) using the entire data set. The dot-dashed lines represent an uncertainty of $\pm 10\%$ around the magenta line.

we utilize them to evaluate the strengths (weaknesses) of the proposed MLE-based structure function estimation approach. As before, we randomly selected 100 subsets of varying sample sizes for both empirical and MLE-based moment estimations. We consider the S_6 values based on Eq. (1) using the entire data set as the "truth."

For small sample sizes, the conventional estimates are quite uncertain (middle panels of Figs. 9 and 10). In addition, for such cases, the median S_6 estimates are significantly outside the $\pm 10\%$ uncertainty bound. In contrast, the MLE-based estimates offer low uncertainty for all sample sizes (right panels of Figs. 9 and 10). For the large Δt case, the MLE-based median estimates are almost identical to the "true" value for all sample sizes. The performance is somewhat poorer for small Δt. In this case, the MLE-based median values are approximately $\pm 10\%$ lower than the "truth" for all sample sizes. For small sample sizes ($N \leqslant 10^4$), the MLE-based approach unequivocally outperforms the conventional approach. Based on these results, we strongly recommend the geophysical community to utilize the proposed MLE-based approach for analyzing data sets with limited sample size.

VIII. ALTERNATIVE PDF

Throughout this paper, we have demonstrated the strengths of the MLE-based approach to estimate higher-order moments. For this purpose, we needed to make an assumption about the underlying pdf of increments. Given its versatility in capturing pdfs of different shapes and forms [84], we opted to use the NIG pdf.

We acknowledge that the NIG pdf has not been fully vetted by the turbulence research community at large. Thus, its appropriateness to represent velocity and/or scalar increments for diverse types of flows remains to be confirmed. In the recent past, other types of pdfs have been proposed (e.g., Refs. [85–87]), and some of them have already gained popularity. In this section, we would like to find out if our MLE-based moment estimation approach can be utilized in conjunction with another type of pdf.

In this proof-of-concept exercise, we choose to use the log-normal superstatistics (LNSS) pdf [64,87,88] given its strikingly different form compared to the NIG pdf (please refer to Appendix C). First, we generate i.i.d. NIG variates ($\alpha = 1, \beta = 0, \mu = 0, \delta = 1$) of different sample sizes. We then estimate S_6 by utilizing the MLE approach. However, unlike before, we make an (incorrect) assumption that the underlying distribution is governed by the LNSS pdf. The results are shown in Fig. 11. The top-panel plot shows that the difference between the NIG and LNSS pdfs are remarkably small (except near the tails). Visually (without using any metrics), both the pdfs appear to be equally representative of the generated random variates. To magnify the tail estimation, the middle panel shows the pdf multiplied by δu^6, which highlights

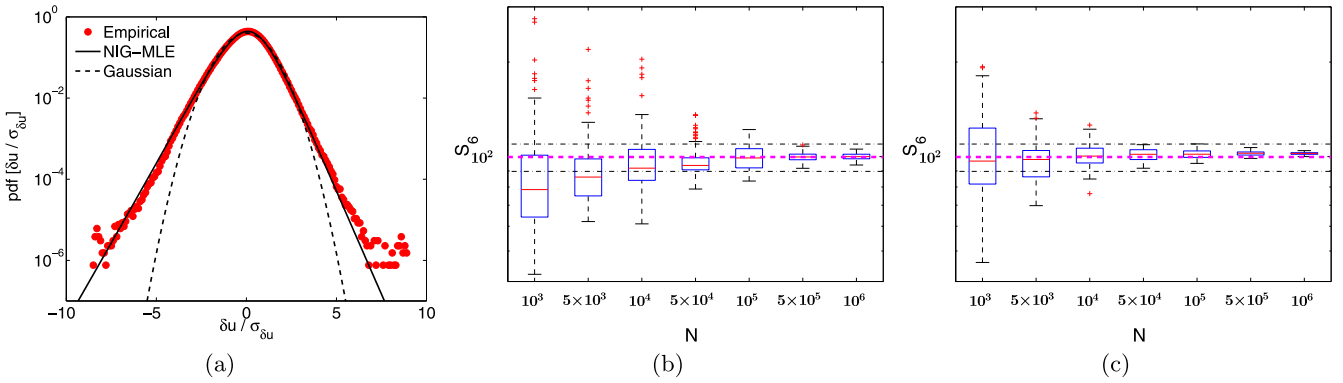

FIG. 10. Same a Fig. 9, except for $r = 277.8$ mm or $\Delta t = 1.35 \times 10^{-2}$ sec.

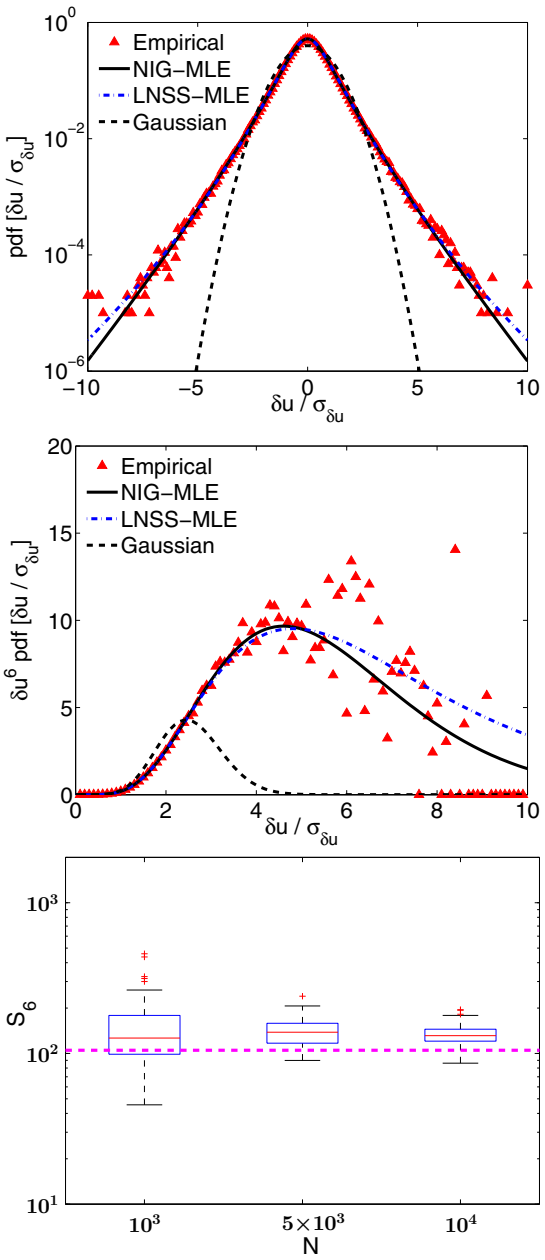

FIG. 11. Top panel: comparison of fitted NIG and LNSS pdfs for i.i.d NIG variates. The sample size is 10^6. Middle panel: magnifies the right-tail estimation by multiplying the pdf by δu^6. Bottom panel: MLE-based S_6 box plot for i.i.d. NIG variates with the (incorrect) assumption of LNSS as the underlying pdf. Due to high computational costs associated with numerical integration of the LNSS pdf, the sample sizes (N) are only limited to 10^4 in this example. The following parameters are utilized to generate the random variates: $\alpha = 1$, $\beta = 0$, $\mu = 0$, and $\delta = 1$. One hundred realizations are used for the construction of the box plot. The dashed magenta line represents the true S_6 value based on Eq. (A4).

the differences in two estimations. More surprisingly, the LNSS-MLE approach overestimates the true S_6 value only by a small margin (see bottom panel of Fig. 11). Undoubtedly, the most important finding is that the estimation bias remains independent of sample size. This result reconfirms the strength of the proposed MLE approach for small sample setting.

IX. CONCLUDING REMARKS

Maximum likelihood estimation (MLE) is an age-old technique and is utilized in countless disciplines. For reasons unknown, the turbulence community has not leveraged on this statistically robust approach for the estimation of higher-order structure functions. In this work, we demonstrate that unbiased estimation of sixth-order structure function with relatively small samples (less than 10^5) is feasible with MLE, whereas the conventional approach fails under these circumstances. Moreover, the unbiasedness of the MLE approach is not affected by correlation within the samples. Last, this approach performs remarkably well for two entirely different types of pdfs: normal inverse Gaussian and log-normal superstatistics. In our future work, we will continue to investigate the prowess of the MLE-based higher-order moment estimation approach by systematically using other observed data sets from turbulence to mesoscale motions. Additionally, we will inter-compare various potential pdf candidates using rigorous metrics (e.g., Kolmogorov-Smirnov and Anderson-Darling).

ACKNOWLEDGMENTS

We are grateful to Yves Gagne for his willingness to share the ONERA wind tunnel data. We would also like to acknowledge Patrick Hawbecker, Avraham Lacser, and the anonymous reviewers for their valuable feedback on this paper. This work was partially funded by the National Science Foundation (AGS–1632679).

APPENDIX A: NORMAL INVERSE GAUSSIAN DISTRIBUTION

The one-dimensional normal inverse Gaussian (NIG) pdf contains four parameters (α, β, δ, and μ) and is defined as follows [89–91]:

$$f_{\mathrm{NIG}}(x;\alpha,\beta,\mu,\delta) = \frac{\alpha}{\pi}\exp(\delta\sqrt{\alpha^2-\beta^2}-\beta\mu)\frac{1}{\sqrt{\phi(x)}} \times \exp(\beta x)K_1[\delta\alpha\sqrt{\phi(x)}], \quad \text{(A1)}$$

where

$$\phi(x) = 1+\left[\frac{x-\mu}{\delta}\right]^2. \quad \text{(A2)}$$

The parameter α controls the steepness of the pdf, where a small α signifies a heavy tail. β is the skewness parameter, such that a negative β indicates that the pdf is skewed to the left. μ is the centrality or translation parameter and is slightly different from the arithmetic mean of the distribution. δ is a scale or peakedness parameter, and it controls the shape of the pdf near its mode. α and δ are always positive, and K_1 is the modified Bessel function of third kind of order one [92].

The parameters of the NIG distribution are explicitly related to the first four central moments [56,74]. Let us denote the sample mean, standard deviation, skewness, and kurtosis by m_1, m_2, m_3, and m_4, respectively. Further define $\gamma = \frac{3}{m_2\sqrt{(3m_4-5m_3^2)}}$. Subsequently, the pdf parameters can be estimated, via the method of moments approach, as

follows [74]:

$$\alpha = \sqrt{\beta^2 + \gamma^2}; \tag{A3a}$$

$$\beta = \frac{(m_2 m_3 \gamma^2)}{3}; \tag{A3b}$$

$$\delta = \frac{m_2^2 \gamma^3}{\beta^2 + \gamma^2}; \tag{A3c}$$

$$\mu = m_1 - \frac{\beta\delta}{\gamma}. \tag{A3d}$$

In this work, without loss of generality, we generated NIG distributed variates with $\mu = 0$ and $\beta = 0$. This choice was made so that Eq. (5) becomes analytically tractable [93] and reduces to

$$S_p = E\left(|x|^p\right) = \frac{2^{\frac{p+1}{2}}\delta^p}{\pi(\alpha\delta)^{\frac{p-1}{2}}} \exp(\alpha\delta)\Gamma\left(\frac{p+1}{2}\right) K_{\frac{p-1}{2}}(\alpha\delta). \tag{A4}$$

For $\alpha = 0.1, \delta = 1$, it is easy to show that $S_6 = 4.965 \times 10^6$. This true value is represented as dashed magenta lines in the left panels of Figs. 2 and 6. True S_6 values using other parameter combinations are also shown in middle and right panels of Figs. 2 and 6.

APPENDIX B: MAXIMUM LIKELIHOOD ESTIMATION

Maximum likelihood estimation (MLE) is a well-established statistical method to estimate the parameters of a given model (say, NIG) which make the sample data, $x_i = x_1, x_2, \ldots, x_N$, the most probable outcome. Let $f(x|\theta)$ denote the underlying NIG pdf of the sample data with parameters θ ($\theta_1 = \alpha, \theta_2 = \beta, \theta_3 = \mu$, and $\theta_4 = \delta$). In the case of independent, identically distributed NIG variates, $f(x|\theta)$ can then be expressed as a joint probability function:

$$f(x|\theta) = f_1(x_1|\theta) f_2(x_2|\theta) \cdots f_N(x_N|\theta). \tag{B1}$$

However, in order to determine the model parameters based on observed data, we have to solve an inverse problem. The first step is to define a likelihood function, where the parameters are a function of the fixed data, as follows:

$$L(\theta|x) = f(x|\theta). \tag{B2}$$

In the case of the NIG pdf, this likelihood function is simply a four-dimensional surface sitting above a four-dimensional hyperplane covering the NIG parameters. For computational ease, it is customary to maximize the log-likelihood (instead of L) to obtain the MLE estimates. The log-likelihood function for the NIG pdf can be written as

$$\begin{aligned}\ln[L(\theta|x)] &= -N\ln(\pi) + N\ln(\alpha) + N(\delta\gamma - \beta\mu) \\ &\quad - \frac{1}{2}\sum_{i=1}^{N}\ln(\phi(x_i)) + \beta\sum_{i=1}^{N}x_i + \sum_{i=1}^{N}\ln\{K_1[\delta\alpha\sqrt{\phi(x_i)}]\},\end{aligned} \tag{B3}$$

where N is the sample size. Next, to find the parametric values which "maximizes" the log-likelihood function, we impose

$$\frac{\partial \ln[L(\theta|x)]}{\partial\theta_k} = 0, \tag{B4}$$

$$\frac{\partial^2 \ln[L(\theta|x)]}{\partial\theta_k^2} < 0, \tag{B5}$$

where k varies from 1 to 4.

Karlis [74] developed an expectation-maximization algorithm to easily maximize Eq. (B3). He leveraged on the fact that the partial derivative of $\ln(L)$ with respect to β leads to a simple relationship connecting the sample mean ($\overline{x}$) and some of the NIG parameters:

$$\overline{x} = \mu + \frac{\delta\beta}{\gamma}. \tag{B6}$$

He also derived the relationships between the conditional expectations of the inverse Gaussian (IG) distribution and NIG parameters (see Ref. [74] for details). A pseudocode for his approach is provided below:

Algorithm 1: Expectation-Maximization for NIG pdf

Initialize:
NIG parameters $(\alpha^{(1)}, \beta^{(1)}, \mu^{(1)}, \delta^{(1)})$ using the MME approach
Compute:
$\ln(L^{(1)})$ using Eq. (B3) and initialized parameters
for $k = 1$ to $k_{\max}$ **do**
Compute:
E-Step - The conditional expectations, s_i and w_i

$$s_i \leftarrow \frac{\delta^{(k)}\sqrt{\phi^{(k)}(x_i)}}{\alpha^{(k)}} \frac{K_0(\delta^{(k)}\alpha^{(k)}\sqrt{\phi^{(k)}(x_i)})}{K_1(\delta^{(k)}\alpha^{(k)}\sqrt{\phi^{(k)}(x_i)})}$$

$$w_i \leftarrow \frac{\alpha^{(k)}}{\delta^{(k)}\sqrt{\phi^{(k)}(x_i)}} \frac{K_{-2}(\delta^{(k)}\alpha^{(k)}\sqrt{\phi^{(k)}(x_i)})}{K_{-1}(\delta^{(k)}\alpha^{(k)}\sqrt{\phi^{(k)}(x_i)})}$$

Compute:
M-Step - Update the parameters using s_i and w_i from previous step

$$\overline{s} \leftarrow \sum_{i=1}^{N}\frac{s_i}{N}$$

$$\widehat{M} \leftarrow \overline{s}$$

$$\widehat{\Lambda} \leftarrow \frac{N}{\sum_{i=1}^{N}(w_i - \frac{1}{\widehat{M}})}$$

$$\delta^{(k+1)} \leftarrow \sqrt{\widehat{\Lambda}}$$

$$\gamma^{(k+1)} \leftarrow \frac{\delta^{(k+1)}}{\widehat{M}}$$

$$\beta^{(k+1)} \leftarrow \frac{\sum_{i=1}^{N}x_i w_i - \overline{x}\sum_{i=1}^{N}w_i}{N - \overline{s}\sum_{i=1}^{N}w_i}$$

$$\mu^{(k+1)} \leftarrow \overline{x} - \beta^{(k+1)}\overline{s}$$

$$\alpha^{(k+1)} \leftarrow \sqrt{(\gamma^{(k+1)})^2 + (\beta^{(k+1)})^2}$$

$i = 1, \ldots, N$
Compute:
$\ln(L^{(k+1)})$ using Eq. (B3) with updated parameters
if $|\frac{\ln(L^{(k+1)}) - \ln(L^{(k)})}{\ln(L^{(k)})}| < 10^{-10}$ **then**
break
end if
end for

APPENDIX C: LOG-NORMAL SUPERSTATISTICS

The concept of superstatistics (a.k.a. "statistics of a statistics") was proposed by Beck and Cohen [87]. The log-normal superstatistics (LNSS) pdf can be written as

$$f_{LNSS}(x;\mu,s) = \frac{1}{2\pi s}\int_0^\infty b^{-1/2}\exp\left\{\frac{-[\ln(b/\mu)]^2}{2s^2}\right\}e^{-(1/2)bx^2}db. \tag{C1}$$

The noncentral second-order moment and the flatness of this distribution can be written as follows [64]:

$$\langle x^2\rangle = \sqrt{w}/\mu, \tag{C2a}$$

$$F_2 = \frac{\langle x^4\rangle}{\langle x^2\rangle^2} = 3w, \tag{C2b}$$

where $w = e^{s^2}$. These equations are easily solved to estimate the unknown parameters μ and s. In the present work, these method of moments-based estimates are used as initial conditions for the MLE computations. A commercial MLE function from MATLAB, employing the Nelder-Mead method, is utilized.

[1] C. W. Van Atta and W. Y. Chen, J. Fluid Mech. **44**, 145 (1970).
[2] A. N. Kolmogorov, Dokl. Akad. Nauk SSSR **30**, 299 (1941).
[3] A. M. Obukhov, Dokl. Akad. Nauk SSSR **32**, 22 (1941).
[4] C. H. Gibson, G. R. Stegen, and S. McConnell, Phys. Fluids **13**, 2448 (1970).
[5] R. W. Stewart, J. R. Wilson, and R. W. Burling, J. Fluid Mech. **41**, 141 (1970).
[6] J. C. Wyngaard and H. Tennekes, Phys. Fluids **13**, 1962 (1970).
[7] C. W. Van Atta and J. Park, in *Statistical Models and Turbulence*, edited by M. Rosenblatt and C. Van Atta, Lecture Notes in Physics (Springer, Berlin, Heidelberg, 1972), Vol. 12, pp. 402–426.
[8] H. Tennekes and J. C. Wyngaard, J. Fluid Mech. **55**, 93 (1972).
[9] R. A. Antonia, B. R. Satyaprakash, and A. J. Chambers, Phys. Fluids **25**, 29 (1982).
[10] K. R. Sreenivasan and B. Dhruva, Prog. Theor. Phys. Suppl. **130**, 103 (1998).
[11] L. Seuront, F. Schmitt, Y. Lagadeuc, D. Schertzer, and S. Lovejoy, J. Plankton Res. **21**, 877 (1999).
[12] S. Lovejoy, W. J. S. Currie, Y. Tessier, M. R. Claereboudt, E. Bourget, J. C. Roff, and D. Schertzer, J. Plankton Res. **23**, 117 (2001).
[13] V. Carbone, Europhys. Lett. **27**, 581 (1994).
[14] T. S. Horbury and A. Balogh, Nonlin. Proc. Geophys. **4**, 185 (1997).
[15] E. Marsch and C.-Y. Tu, Nonlin. Proc. Geophys. **4**, 101 (1997).
[16] J. J. Podesta, M. A. Forman, C. W. Smith, D. C. Elton, Y. Malécot, and Y. Gagne, Nonlin. Proc. Geophys. **16**, 99 (2009).
[17] C. Salem, A. Mangeney, S. D. Bale, and P. Veltri, Astrophys. J. **702**, 537 (2009).
[18] J. Delour, J. F. Muzy, and A. Arneodo, Euro. Phys. J. B **23**, 243 (2001).
[19] B. Castaing, Euro. Phys. J. B **29**, 357 (2002).
[20] A. Arnéodo, R. Benzi, J. Berg, L. Biferale, E. Bodenschatz, A. Busse, E. Calzavarini, B. Castaing, M. Cencini, L. Chevillard, *et al.*, Phys. Rev. Lett. **100**, 254504 (2008).
[21] F. Toschi and E. Bodenschatz, Annu. Rev. Fluid Mech. **41**, 375 (2009).
[22] R. H. Kraichnan, Phys. Rev. Lett. **72**, 1016 (1994).
[23] P. Constantin, J. Stat. Phys. **90**, 571 (1998).
[24] A. Celani, M. Cencini, A. Mazzino, and M. Vergassola, New J. Phys. **6**, 72 (2004).
[25] K. G. Aivalis, K. R. Sreenivasan, Y. Tsuji, J. C. Klewicki, and C. A. Biltoft, Phys. Fluids **14**, 2439 (2002).
[26] I. Mazzitelli and A. S. Lanotte, Physica D (Amsterdam) **241**, 251 (2012).
[27] B. Castaing, G. Gunaratne, L. Kadanoff, A. Libchaber, and F. Heslot, J. Fluid Mech. **204**, 1 (1989).
[28] V. Yakhot, Phys. Rev. Lett. **69**, 769 (1992).
[29] R. Benzi, R. Tripiccione, F. Massaioli, S. Succi, and S. Ciliberto, Europhys. Lett. **25**, 341 (1994).
[30] L. Skrbek, J. J. Niemela, K. R. Sreenivasan, and R. J. Donnelly, Phys. Rev. E **66**, 036303 (2002).
[31] D. Lohse and K.-Q. Xia, Annu. Rev. Fluid Mech. **42**, 335 (2010).
[32] U. Frisch, *Turbulence* (Cambridge University Press, Cambridge, 1995), p. 296.
[33] A. Tsinober, *An Informal Introduction to Turbulence* (Kluwer Academic Publishers, Dordrecht, 2001), Vol. 63.
[34] E. A. Novikov and R. W. Stewart, Izv. Geophys. Ser. **3**, 408 (1964).
[35] U. Frisch, P.-L. Sulem, and M. Nelkin, J. Fluid Mech. **87**, 719 (1978).
[36] B. B. Mandelbrot, in *Statistical Models and Turbulence*, edited by M. Rosenblatt and C. Van Atta, Lecture Notes in Physics (Springer, Berlin, Heidelberg, 1972), Vol. 12, pp. 333–351.
[37] R. Benzi, G. Paladin, G. Parisi, and A. Vulpiani, J. Phys. A **17**, 3521 (1984).
[38] U. Frisch and G. Parisi, in *Turbulence and Predictability in Geophysical Fluid Dynamics and Climate Dynamics*, edited by M. Ghil, R. Benzi, and G. Parisi (North-Holland Publ. Co., Amsterdam, 1985), pp. 71–88.
[39] E. N. Lorenz, J. Fluid Mech. **55**, 545 (1972).
[40] K. Ohkitani and M. Yamada, Prog. Theor. Phys. **81**, 329 (1989).
[41] M. H. Jensen, G. Paladin, and A. Vulpiani, Phys. Rev. A **43**, 798 (1991).
[42] E. S. C. Ching and W. C. Cheng, Phys. Rev. E **77**, 015303 (2008).
[43] S. Basu, J. Turbul. **10**, 1 (2009).
[44] V. R. Kuznetsov and V. A. Sabel'nikov, *Turbulence and Combustion* (Hemisphere Publishing, New York, 1990), p. 362.
[45] G. C. Burton and W. J. A. Dahm, Phys. Fluids **17**, 075112 (2005).

[46] A. Morales, M. Wächter, and J. Peinke, Wind Energy **15**, 391 (2012).
[47] H. F. C. Velho, R. R. Rosa, F. M. Ramos, R. A. Pielke, G. A. Degrazia, C. R. Neto, and A. Zanandrea, Physica A (Amsterdam) **295**, 219 (2001).
[48] F. N. Frenkiel and P. S. Klebanoff, Bound.-Lay. Meteorol. **8**, 173 (1975).
[49] F. Anselmet, Y. Gagne, E. J. Hopfinger, and R. A. Antonia, J. Fluid Mech. **140**, 63 (1984).
[50] A. Vincent and M. Meneguzzi, J. Fluid Mech. **225**, 1 (1991).
[51] L. Zubair, *Studies in Turbulence using Wavelet Transforms for Data Compression and Scale Separation*, Ph.D. thesis, Yale University (1993).
[52] F. Schmitt, D. Schertzer, S. Lovejoy, and Y. Brunet, Nonlin. Proc. Geophys. **1**, 95 (1994).
[53] F. Belin, P. Tabeling, and H. Willaime, Physica D (Amsterdam) **93**, 52 (1996).
[54] W. van de Water and J. A. Herweijer, J. Fluid Mech. **387**, 3 (1999).
[55] J. M. Vindel, C. Yagüe, and J. M. Redondo, Nonlin. Proc. Geophys. **15**, 915 (2008).
[56] O. E. Barndorff-Nielsen, P. Blæsild, and J. Schmiegel, Eur. Phys. J. B **41**, 345 (2004).
[57] G. J. Kunkel and I. Marusic, J. Fluid Mech. **548**, 375 (2006).
[58] I. Marusic and G. J. Kunkel, Phys. Fluids **15**, 2461 (2003).
[59] S. Basu, E. Foufoula-Georgiou, B. Lashermes, and A. Arnéodo, Phys. Fluids **19**, 115102 (2007).
[60] T. H. Rydberg, Commun. Stat. Stochastic Models **13**, 887 (1997).
[61] E. Marsch and C.-Y. Tu, Ann. Geophys. **12**, 1127 (1994).
[62] K. R. Sreenivasan and R. A. Antonia, Annu. Rev. Fluid Mech. **29**, 435 (1997).
[63] L. Sorriso-Valvo, V. Carbone, P. Veltri, G. Consolini, and R. Bruno, Geophys. Res. Lett. **26**, 1801 (1999).
[64] C. Beck, Physica D (Amsterdam) **193**, 195 (2004).
[65] R. Calif and F. G. Schmitt, J. Wind Eng. Ind. Aerodyn. **109**, 1 (2012).
[66] T. Dudok de Wit, Phys. Rev. E **70**, 055302(R) (2004).
[67] P. Embrechts, C. Klüppelberg, and T. Mokosh, *Modelling Extremal Events for Insurance and Finance* (Springer-Verlag, Berlin, Heidelberg, 1997), p. 648.
[68] J. Pickands, III, Ann. Stat. **3**, 119 (1975).
[69] B. M. Hill, Ann. Stat. **3**, 1163 (1975).
[70] A. L. M. Dekkers, J. H. J. Einmahl, and L. De Haan, Ann. Stat. **17**, 1833 (1989).
[71] H. Drees, L. De Haan, and S. Resnick, Ann. Stat. **28**, 254 (2000).
[72] It is mathematically more accurate to say that the NIG distributions capture semiheavy tails.
[73] D. Karlis and J. Lillestöl, Appl. Stoch. Model Bus. **20**, 323 (2004).
[74] D. Karlis, Stat. Probabil. Lett. **57**, 43 (2002).
[75] I. J. Myung, J. Math. Psychol. **47**, 90 (2003).
[76] R. B. d'Agostino and M. A. Stephens (eds.) *Goodness-of-Fit Techniques* (Marcel Dekker, New York, 1986).
[77] A. P. Dempster, N. M. Laird, and D. B. Rubin, J. Roy. Stat. Soc. B Met. **39**, 1 (1977).
[78] J. A. Nelder and R. Mead, Comput. J. **7**, 308 (1965).
[79] J. C. Lagarias, J. A. Reeds, M. H. Wright, and P. E. Wright, SIAM J. Optim. **9**, 112 (1998).
[80] Y. Huang, F. G. Schmitt, Z. Lu, and Y. Liu, Europhys. Lett. **86**, 40010 (2009).
[81] H. Kahalerras, Y. Malecot, Y. Gagne, and B. Castaing, Phys. Fluids **10**, 910 (1998).
[82] Y. Malécot, C. Auriault, H. Kahalerras, Y. Gagne, O. Chanal, B. Chabaud, and B. Castaing, Euro. Phys. J. B. Condens. Matt. Complex Syst. **16**, 549 (2000).
[83] Y. Gagne, B. Castaing, C. Baudet, and Y. Malécot, Phys. Fluids **16**, 482 (2004).
[84] A. Eriksson, E. Ghysels, and L. Forsberg, *Approximating the Probability Distribution of Functions of Random Variables: A New Approach* (Working Paper, CIRANO, Montreal, 2004), p. 22.
[85] B. Castaing, Y. Gagne, and E. J. Hopfinger, Physica D (Amsterdam) **46**, 177 (1990).
[86] P. Kailasnath, K. R. Sreenivasan, and G. Stolovitzky, Phys. Rev. Lett. **68**, 2766 (1992).
[87] C. Beck and E. Cohen, Physica A (Amsterdam) **322**, 267 (2003).
[88] C. Beck, E. Cohen, and S. Rizzo, Europhys. News **36**, 189 (2005).
[89] O. Barndorff-Nielsen, Proc. Roy. Soc. London A **353**, 401 (1977).
[90] M. Paolella, *Intermediate Probability: A Computational Approach* (John Wiley & Sons, Hoboken, NJ, 2007).
[91] D. J. Scott, D. Würtz, C. Dong, and T. T. Tran, Comput. Stat. **26**, 459 (2011).
[92] M. Abramowitz and I. A. Stegun, *Handbook of Mathematical Functions: With Formulas, Graphs, and Mathematical Tables* (Dover, New York, 1972).
[93] O. E. Barndorff-Nielsen and R. Stelzer, Scand. J. Stat. **32**, 617 (2005).